Supporting Information

Approaching a Minimal Topological Electronic Structure in Antiferromagnetic Topological Insulator MnBi₂Te₄ via Surface Modification

Aiji Liang[1,2*], Cheng Chen[3*], Huijun Zheng[1], Wei Xia[1,2], Kui Huang[1], Liyang Wei[1], Haifeng Yang[1], Yujie Chen[4], Xin Zhang[1], Xuguang Xu[1,2], Meixiao Wang[1,2], Yanfeng Guo[1,2], Lexian Yang[4,5], Zhongkai Liu[1,2‡], Yulin Chen[1,2,3,4‡]

[1]*School of Physical Science and Technology, ShanghaiTech University, Shanghai 201210, China*

[2]*ShanghaiTech Laboratory for Topological Physics, Shanghai 200031, P. R. China*

[3]*Clarendon Laboratory, Department of Physics, University of Oxford, Oxford OX1 3PU, U.K.*

[4]*State Key Laboratory of Low Dimensional Quantum Physics, Department of Physics, Tsinghua University, Beijing 100084, China*

[5]*Frontier Science Center for Quantum Information, Beijing 100084, China*

*Aiji Liang and Cheng Chen contributed equally in the work.

Corresponding Authors

Zhongkai Liu. E-mail: liuzhk@shanghaitech.edu.cn

Yulin Chen. E-mail: yulin.chen@physics.ox.ac.uk

1. Laser circular dichroism of MnBi$_2$Te$_4$

As a complementary of Figure 1 in main text, we show laser circular dichroism (CD) of MnBi$_2$Te$_4$ measured along $\overline{\Gamma}$-$\overline{M}$ (measured at ~80K) in Figure S1. The CD contrast pattern (Fig. S1d) is similar to that in Fig. 1g, especially the clear blue and red contrast between SS1 and SS2.
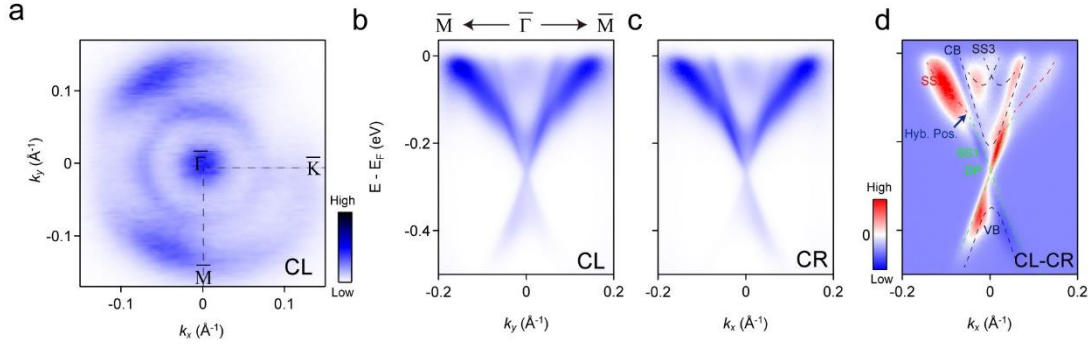

Figure S1. Laser circular dichroism (CD) of MnBi$_2$Te$_4$ measured along $\overline{\Gamma}$-$\overline{M}$. (a) Fermi surface measured by circular left (CL) polarized photons along $\overline{\Gamma}$-$\overline{M}$. (b, c) Band dispersions along $\overline{\Gamma}$-$\overline{M}$ measured by CL and circular right (CR) polarized photons. (d) CD image obtained by the difference (CL-CR) of those in (b, c). The dashed curves are guides for eyes.

2. Volume of K dosing dependent band structure of MnBi$_2$Te$_4$ by laser-based ARPES

In Figure S2, we demonstrate further analysis of K dosing data by laser-based ARPES in the main text Figure 2. Some key energy changes of bulk and surface states upon K dosing are extracted. Surface states and bulk bands show very different response upon K dosing (see the extracted curves in Fig. S2c). The hybridization position between TSS and RSS get closer to Dirac point (DP) upon K dosing, as the energy difference between hybridization position and DP decreases (Fig. S2d, triangle black curve). Moreover, the hybridization position between TSS and RSS and the bottom of SS3 have almost equal energetic shift upon K dosing before the critical K dosing (Fig. S2d, red curve), which supports the TSS and RSS hybridization picture.
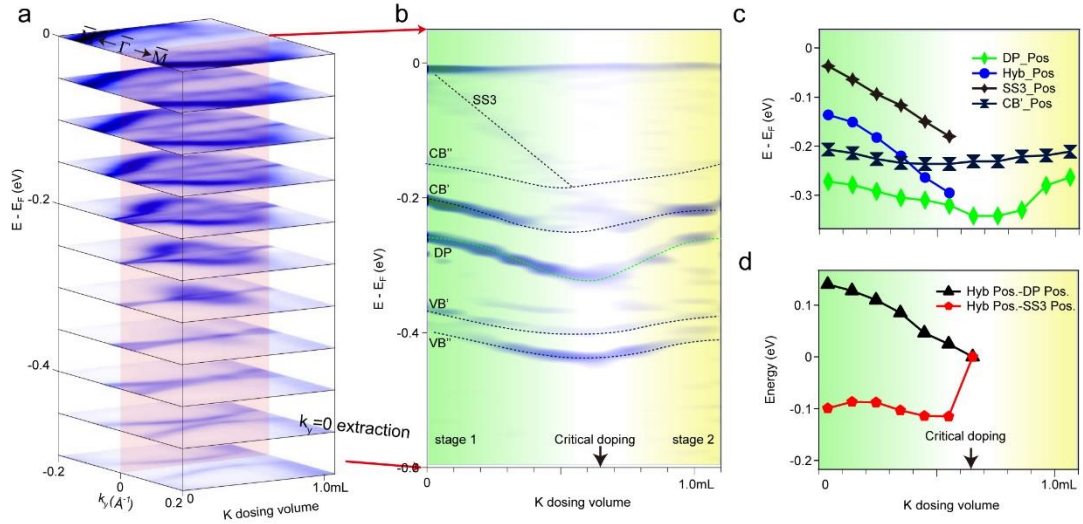
Figure S2. Volume of K dosing dependent band structure of MnBi$_2$Te$_4$ by laser-based ARPES.

(a) A stack plot of constant energy contours to demonstrate electronic structure evolution upon K dosing. (b) A curvature plot of energy distribution curves (EDCs) along k_y=0 plane in (a). (c) Energy position changing of DP, Hyb. Pos., bottom of SS3 and bottom of CB' upon K dosing are extracted from (b) and Fig. 2 in main text. (d) The energy difference of Hyb. Pos. and DP, Hyb. Pos. and bottom of SS3 upon K dosing.

3. **Temperature dependent conduction band splitting of pristine and massive K dosed MnBi$_2$Te$_4$**

In Figure S3, the original EDCs in correspondence to those in main text Figs. 3d and h. (temperature dependent conduction band measured from pristine and massive K dosed MnBi$_2$Te$_4$) are exhibited. The closing temperature of conduction band splitting in both cases is the same, which is at ~28K.
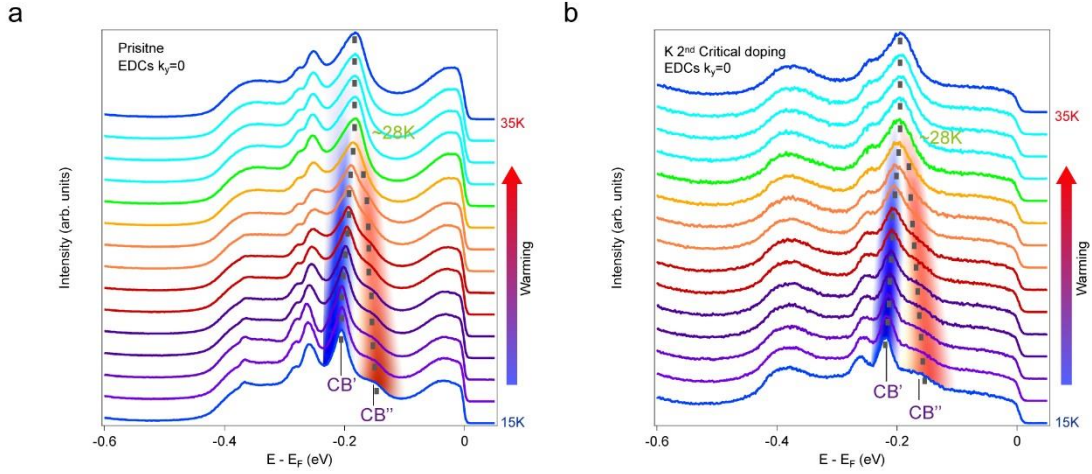
Figure S3. Original EDCs of temperature dependent conduction band splitting of pristine and massive K dosed MnBi$_2$Te$_4$. (a) Pristine. (b) Massive K dosed in stage 2. They are in correspondence to those in Figs. 3 d and h. of main text.

4. Volume of K dosing dependent band structure of MnBi$_2$Te$_4$ by synchrotron-based ARPES

Volume of K dosing dependent band structure and core levels of MnBi$_2$Te$_4$ are demonstrated in Figure S4, which resembles to those in Figure 2 (band structure) and is a complementary of Figure 4 (core levels) in main text. K dosing dependent band structure (Figs. S4 a-m) and core levels of Te 4d, Bi 5d and K 3p (Figs. S4n-o) are measured in each round. Mn 3s state is also measured (Fig. S4p). The vanish of trivial surface state SS2 happens roughly in Fig. S4f (K dosing sequence 6), which is the hallmark to distinguish stage 1 and 2. The bulk K 3p state appears in companion with less oxidized Bi 5d side peaks in the sixth dosing (Fig. S4o), where the trivial surface state SS2 is killed at the same time (Fig. S4f). Such coincidence can be explained by the forming of K clusters resulted in simultaneous K-Te-Bi alloying [1-4]. Both processes lead to a trapping and reduction of

free charge carriers and surface chemical potential moves downwards showing hole doping. Moreover, the randomly distributed K clusters and K-Te-Bi alloying modify surface potential dramatically such that surface potential translational periodic symmetry is broken. The very surface localized trivial surface state SS2 is thus killed. Notice that, side peaks of Mn 3s are not observed during the whole K dosing process (Fig. S4p). This is natural, since Mn atoms are buried deeper in the bulk, implying that the alloying effect mentioned above is mainly localized at the very surface.

Though, the deposited K atoms do not show ordering, we could still adopt the idea that the development of an extra K 3P core level state is a rough point to define the transition from the first layer to the second one (bulk like) [5]. As the clean and complete disappearance of RSS is coincident with the development of bulk like extra K 3p core level (Figs. S4f, g and o), we can define the volume of K atoms of sixth dosing roughly to be the first monolayer. Bearing in mind that the very similar volume of K dosing dependent band structure between synchrotron-based ARPES data in Figure S4 and that of laser-based ARPES data in main text Figure 2, we can in return, give an estimation of K atoms coverage of each round shown in main text Figure 2, where the first round of clean and complete suppression of RSS (No. 10 or No. 11 K dosing in main text Fig. 2a) to be the volume of K dosing within a full coverage of a mono-layer (ML).
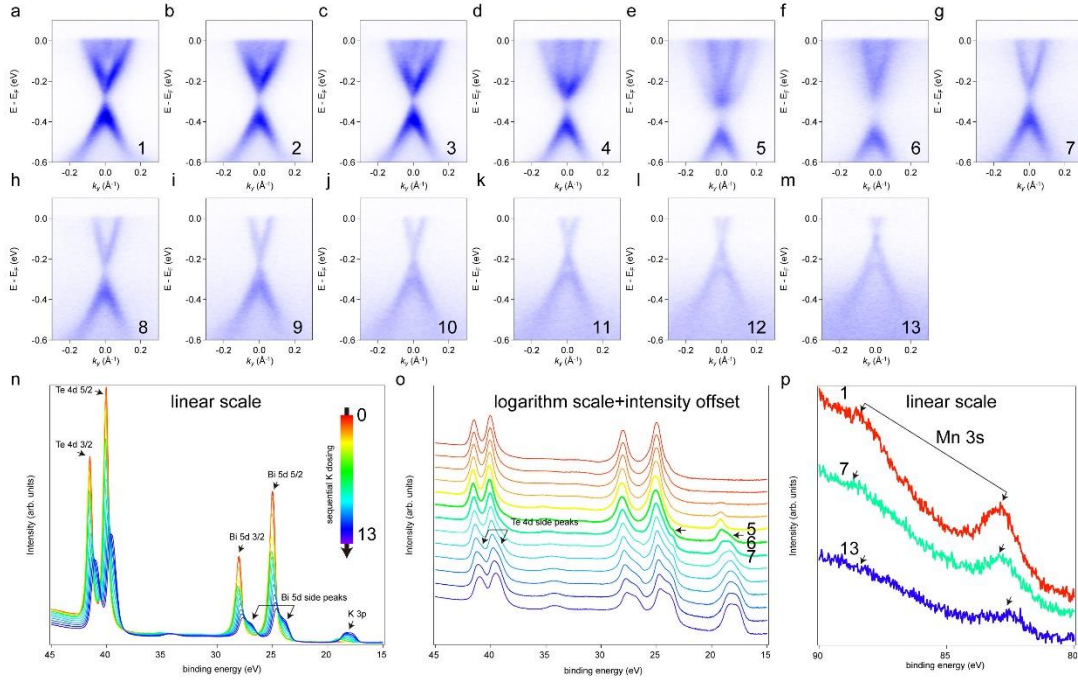
Figure S4. Volume of K dosing dependent band structure of MnBi$_2$Te$_4$ by synchrotron-based ARPES. (a-m) Sequential K dosing dependent band structure of MnBi$_2$Te$_4$ along $\bar{\Gamma}$-$\bar{M}$. (n-o) Core levels of Te 4d, Bi 5d and K 3p in correspondence to those in (a-m). The core level intensity shows with linear scale in (n) and logarithm scale with offset in (o). (p) Core levels of Mn 3s. The measuring time order is also noted.

5. Schematic of back gate on massive K dosed MnBi$_2$Te$_4$ film

The bottom of conduction band is about ~0.05eV (Fig. S4m) beneath Fermi level in comparison to ~0.25eV (Fig. S4a) beneath Fermi level for the pristine case as schematically illustrated in Figs. S5b-c. The reduced bulk carriers are desired for transport measurement. In the follow-up work, we performed the same K dosing experiment on MBE grown MnBi$_2$Te$_4$ films and observed similar trend of band evolution until we greatly approached the "minimal" electronic structure of an MTI (Xu, R. Z.; et al., unpublished experiments). Therefore, with proper

K dosing level (Fig. S4m), as well as a certain amount of electrostatic field (e.g. by back-gating the sample, Figs. S5a), it is possible to tune the Fermi level to the bulk gap, even close to the Dirac point (Fig. S5d) and observe the predicted quantum transport effects. The K dosed sample has much smaller carrier concentrations (Fig. S4m and Fig. S5c) and is thus much easier for the electrostatic gating, which may be important for transport research as well as future applications.
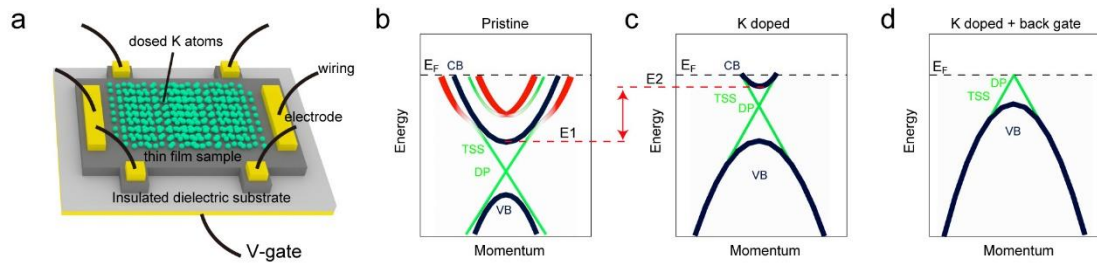

Figure S5. **Schematic of back gate on massive K dosed MnBi$_2$Te$_4$ film.** (a) Schematic of MnBi$_2$Te$_4$ thin film device with potassium dosage and electrostatic back gate. (b) Illustration of the electronic structure of pristine thin film of MnBi$_2$Te$_4$. E1 marks the binding energy of the conduction band bottom. (c) Illustration of the electronic structure of K dosed thin film MnBi$_2$Te$_4$. E2 marks the binding energy of the conduction band bottom. E2 is ~1/5 of E1, easier for back gate in massive K doped case. (d) Illustration of the electronic structure with K dosed and gated thin film MnBi$_2$Te$_4$. All the band labels are the same to Figure. 1 in the manuscript.

6. Volume of K dosing dependent band structure of MnBi$_2$Te$_4$ after annealing

K dosing volume dependent band structure of MnBi$_2$Te$_4$ after annealing is demonstrated in Figure S6. When volume of K dosing is small (Fig. S6b) that interfacial interaction between K atoms and sample surface dominates, the effect brought by K dosing to band structure, especially surface states,

can be fully removed by warming up the sample to room temperature. The cooling back band structure (Fig. S6c) then almost recovers to the pristine state (Fig. S6a). This is likely due to the escaping of movable K atoms. When the volume of K dosing is large enough (Fig. S6e) that mutual interactions between K atoms prevail over interfacial interaction and trivial surface state SS2 is killed, the band structure cannot recover back to pristine state by a simple sample warming and cooling back (Fig. S6f). The warming leads to more K-Te-Bi alloying in massive K dosed sample, chemical potential moves downwards more (Fig. S6f).
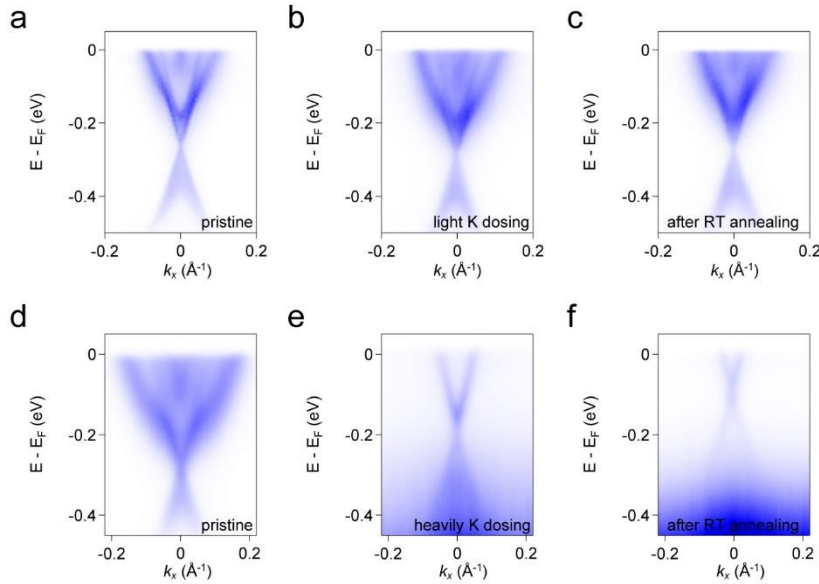

Figure S6. Volume of K dosing dependent band structure of MnBi$_2$Te$_4$ after annealing. (a) band structure of pristine MnBi$_2$Te$_4$ along $\bar{\Gamma}$-$\bar{K}$ at ~80K. (b) Band structure taken after light volume of K dosing of (a). (c) Band structure taken after warming up sample temperature to ~300K (RT) for 5min and cooling back to ~80K. (d-f) Same procedure to those in (a-c), except on a massive K dosed sample. Note that the intrinsic doping level of the two samples show some difference.

References:

[1] Scholz, M. R.; Sánchez-Barriga, J.; Marchenko, D.; Varykhalov, A.; Volykhov, A.; Yashina, L. V.; Rader, O. Tolerance of Topological Surface States towards Magnetic Moments: Fe on Bi_2Se_3. *Phys Rev Lett* **2012,** 108, (25), 256810. DOI: 10.1103/PhysRevLett.108.256810.

[2] Vondráček, M.; Cornils, L.; Minár, J.; Warmuth, J.; Michiardi, M.; Piamonteze, C.; Barreto, L.; Miwa, J. A.; Bianchi, M.; Hofmann, P.; Zhou, L.; Kamlapure, A.; Khajetoorians, A. A.; Wiesendanger, R.; Mi, J. L.; Iversen, B. B.; Mankovsky, S.; Borek, S.; Ebert, H.; Schüler, M.; Wehling, T.; Wiebe, J.; Honolka, J. Nickel: The time-reversal symmetry conserving partner of iron on a chalcogenide topological insulator. *Phys Rev B* **2016,** 94, (16), 161114. DOI: 10.1103/PhysRevB.94.161114.

[3] Ferfolja, K.; Fanetti, M.; Gardonio, S.; Panighel, M.; Pis, I.; Nappini, S.; Valant, M. A cryogenic solid-state reaction at the interface between Ti and the Bi_2Se_3 topological insulator. *J Mater Chem C* **2020,** 8, (33), 11492-11498. DOI: 10.1039/d0tc00863j.

[4] Cui, J.; Zheng, H.; Zhang, Z.; Hwang, S.; Yang, X.-Q.; He, K. Origin of anomalous high-rate Na-ion electrochemistry in layered bismuth telluride anodes. *Matter* **2021,** 4, (4), 1335-1351. DOI: https://doi.org/10.1016/j.matt.2021.01.005.

[5] Kim, Y. K.; Krupin, O.; Denlinger, J. D.; Bostwick, A.; Rotenberg, E.; Zhao, Q.; Mitchell, J. F.; Allen, J. W.; Kim, B. J. Fermi arcs in a doped pseudospin-1/2 Heisenberg antiferromagnet. *Science* **2014,** 345, (6193), 187-190. DOI: 10.1126/science.1251151.